The Journal of Chemical Physics

RESEARCH ARTICLE | DECEMBER 05 2024

Recasting the wobbling-in-a-cone model for the rotational anisotropy of phenylselenocyanate in poly(methyl methacrylate): Effect of internal bond rotation and polymer segmental motion

Special Collection: David Jonas Festschrift

Sourav Palchowdhury ; Saptarsi Mondal ; Kyungwon Kwak ; Minhaeng Cho

J. Chem. Phys. 161, 214112 (2024)
https://doi.org/10.1063/5.0239896

The Journal of Chemical Physics ARTICLE pubs.aip.org/aip/jcp

Recasting the wobbling-in-a-cone model for the rotational anisotropy of phenylselenocyanate in poly(methyl methacrylate): Effect of internal bond rotation and polymer segmental motion

Cite as: J. Chem. Phys. 161, 214112 (2024); doi: 10.1063/5.0239896
Submitted: 23 September 2024 • Accepted: 17 November 2024 •
Published Online: 5 December 2024

Sourav Palchowdhury,[1,2] Saptarsi Mondal,[1,2] Kyungwon Kwak,[1,2,a)] and Minhaeng Cho[1,2,a)]

AFFILIATIONS

[1] Center for Molecular Spectroscopy and Dynamics, Institute for Basic Science (IBS), Seoul 02841, Republic of Korea
[2] Department of Chemistry, Korea University, Seoul 02841, Republic of Korea

Note: This paper is part of the JCP Special Topic, David Jonas Festschrift.
[a)] **Author to whom correspondence should be addressed:** mcho@korea.ac.kr

ABSTRACT

The rotational anisotropy of a molecule in a constrained environment is modeled by wobbling-in-a-cone (WIAC) motion, which describes the angular space sampled by the molecule. Recent polarization-selective IR pump–probe measurements have applied this model to phenylselenocyanate in amorphous polymers, aiming to probe the surrounding free volume. A faster rotational timescale was hypothesized to reflect the angular space within the static voids of the polymer matrix, while a slower timescale relates to constraint release by the polymer backbones. To better quantify the contributions of internal bond rotation and polymer segmental motion, we conduct molecular dynamics simulations on two phenylselenocyanate variants with different internal rotational barriers, as well as on *p*-chlorobenzonitrile, which lacks such internal rotational freedom, within a polymer matrix. Our analyses reveal that the faster (~10 ps) component of the cyano group's anisotropy decay arises from concurrent angular sampling due to internal bond rotation and WIAC motion. Conversely, polymer segmental motion was found to have a minimal influence on the slow (~200 ps) anisotropy component. Based on these findings, we refine the WIAC model to better link rotational diffusion with the distinct free volume elements accessed by the probe molecule. This revised model allows the quantification of free volume elements associated with both internal bond rotation and wobbling motion within the polymer cage.

I. INTRODUCTION

The reorientational relaxation of a molecule in a condensed phase is particularly sensitive to the magnitude and timescale of the friction exerted by the surrounding solvent cage.[1,2] In a low-viscous medium, where the solvent cage is transient, the rotational diffusion of the probe molecule obeys the Stokes–Einstein–Debye (SED) type mechanism, exhibiting a single-exponential decay of its reorientational time correlation function (TCF).[3,4] However, in high-viscous media, such as room-temperature ionic liquids, concentrated electrolyte solutions, and amorphous polymers, the slow dynamics of the solvent molecules result in a long-lasting solvent cage around the probe. This leads to a complex reorientational mechanism for the probe, constrained by the persistence of the cage around the molecule. The restricted rotational motion within such a highly caged environment was first theoretically modeled by the wobbling-in-a-cone (WIAC) motion,[5–7] specifically developed for fluorescence depolarization and nuclear magnetic resonance (NMR) experiments. In this model, the diffusing probe can only sample a limited range of angular space until it encounters the wall of the surrounding solvent cage. Once the cage relaxes, the probe molecule can explore a larger angular cone, determined by the available free space around it.

In recent studies[8,9] using polarization-selective IR pump–probe (PS IR-PP) measurements on the cyano (–CN) chromophore of phenylselenocyanate (PSC), a vibrational probe embedded in

poly(methyl methacrylate) (PMMA), the orientational relaxation process (anisotropy decay) of the probe molecule within the polymer matrix was quantitatively measured by combining the parallel ($I_\parallel$) and perpendicular signals ($I_\perp$),

$$r(t) = \frac{I_\parallel - I_\perp}{I_\parallel + 2I_\perp} = 0.4C_2(t), \tag{1}$$

where $C_2(t)$ is the rotational time correlation function. Their analysis, based on the WIAC model, resulted in a bi-exponential decay with an offset in the reorientational time correlation function,

$$C_2(t) = S_0^2\left\{S_1^2 + \left(1 - S_1^2\right)e^{-t/\tau_1}\right\}\left\{S_2^2 + \left(1 - S_2^2\right)e^{-t/\tau_2}\right\}. \tag{2}$$

The time constants τ_1 and τ_2 were attributed to the orientational decay of the probe molecule inside the persistent cage (first diffusive cone) and the process of releasing the cage constraint due to the polymer's segmental motions (second diffusive cone). Their fitting analysis of the experimentally measured $C_2(t)$ yielded τ_1 and τ_2 time constants of ~10 and ~200 ps, respectively. The amplitude factors S_0^2, S_1^2, and S_2^2 are the order parameters associated with the motion of the probe due to ultrafast inertial dynamics, dynamics within the first diffusive cone, and dynamics within the second diffusive cone, respectively.

The cone half-angles (θ_i) sampled by the probe molecule within the free volume element (FVE) of the polymer matrix are related to the extracted order parameters by the following equation:

$$S_i = \frac{1}{2}\cos(\theta_i)(1 + \cos(\theta_i)). \tag{3}$$

Here, θ_0, θ_1, and θ_2 are the half-cone angles sampled by the probe molecule, corresponding to the reorientational mechanism described by the WIAC model. The effective half-cone angle θ_{0+1}, derived from the cumulative order parameter S_0S_1, represents the angular space sampled using the vibrational probe within the static FVE of the polymer. The total angular space sampled after the constraint is released, which is described by θ_{tot} from the cumulative order parameter $S_0S_1S_2$, corresponds to coupling with the polymer segmental motion. These half-cone angles can be related to the cylindrical FVE around the probe using

$$r_i = a\sin(\theta_i) + \Delta r, \tag{4}$$

where r_i is the radius of the base of the cylindrical FVE, Δr is the van der Waals radius of the most distant atom from the center-of-mass (COM) of the probe molecule (para-hydrogen in the case for PSC with a value of 1.2 Å), and a is the distance of that atom from the center-of-mass (3.15 Å for PSC). Assuming θ_{0+1} to be the half-cone angle sampled by PSC within the static FVE, $\langle r\rangle$ was calculated to be ~3.0 Å, in excellent agreement with values reported by positron annihilation lifetime spectroscopy (PALS).[10]

PSC, characterized by a bend around the C_{Ph}–C_{Ph}–Se–CN dihedral, can undergo internal bond rotation, contributing to the rotational anisotropy decay of the –CN bond vector independent of the WIAC motion within the FVE. To account for this, a series of –CN containing vibrational probes with varying degrees of internal bond rotation relative to the phenyl ring were subjected to PS IR-PP measurements in a polystyrene polymer matrix.[11] The resulting FVE estimations were consistent across different vibrational probes, confirming the robustness of the method.

In a recent study,[12] we aimed to explore the relationship between the FVE and water permeability in a series of biocompatible polymers with structurally similar yet functionally distinct side chains—PMMA, poly(2-phenoxyethyl acrylate) (PPEA), and poly(2-methoxyethyl acrylate) (PMEA). Analogous PS IR-PP experiments using the PSC probe revealed very similar $\langle\theta_{0+1}\rangle$ values in all three polymers:[12] 22.1° in PMMA, 26.6° in PPEA, and 26.5° in PMEA. This raised the question of whether θ_{0+1} is solely associated with the wobbling motion of PSC within the static FVE of the polymers or whether it also results from similar internal rotation of the –SeCN group around the C_{Ph}–C_{Ph}–Se–CN dihedral.

To investigate this further, we conducted experiments using two additional PSC variants, 2-methylphenylselenocyanate (MPSC) and 2,2-dimethylphenylselenocyanate (DMPSC), embedded in PMMA. These probes differ in the torsional barrier around the C_{Ph}–C_{Ph}–Se–CN dihedral due to the increasing number of ortho-substituted methyl groups. The short-time rotational anisotropy dynamics of the nitrile group was found to be approximately 5–6 times slower in MPSC (28.7 ± 1.4 ps) and DMPSC (31.9 ± 1.8 ps) compared to PSC (4.8 ± 0.5 ps), indicating the significant role of internal rotational fluctuations in anisotropy decay.

Another recent experimental study investigated the influence of internal bond rotation on the anisotropy decay of CN-containing vibrational probes, including *p*-chlorobenzonitrile, phenylthiocyanate, phenylselenocyanate, and 2-nitrophenylselenocyanate, in an *N*,*N*-dimethylformamide (DMF) solvent using PS IR-PP techniques.[13] They found that, except for *p*-chlorobenzonitrile, the other probes exhibited a bi-exponential anisotropy decay. The faster time component was attributed to intramolecular bond rotation around the dihedral connecting the phenyl group to the chromophore, while the slower component was related to the complete randomization of the transition dipole moment vector due to full diffusive molecular reorientation in the low-viscous, minimally caging DMF solvent. *Para*-chlorobenzonitrile, lacking such internal bond rotation, displayed only a single-exponential anisotropy decay attributed to its diffusive molecular reorientation. Applying the WIAC model to the bi-exponential rotational anisotropy decay of the three molecules yielded $\langle\theta_{0+1}\rangle$ values of 29.5 ± 9.9°, 22.3 ± 1.4°, and 22.2 ± 2.1° for phenylthiocyanate, phenylselenocyanate, and 2-nitrophenylselenocyanate, respectively. These values were inversely related to the torsional barrier around the C_{Ph}–C_{Ph}–X–CN (X = S or Se) dihedral. However, it is important to note that the $\langle\theta_{0+1}\rangle$ values for PSC in both DMF and PMMA are nearly identical. This observation underscores the need to quantify the extent of internal bond rotation on the anisotropy decay of PSC to accurately determine the FVE around the probe.

Based on the preceding discussions, we recognize the necessity of directly quantifying the amplitude of internal bond rotation and the effect of solvent cage relaxation on the rotational anisotropy of vibrational probes within a polymer matrix. In this study, we examine the impact of internal bond rotation on the rotational anisotropy of PSC, DMPSC, and *p*-chlorobenzonitrile (ClBZN) probes embedded in the PMMA polymer, using classical molecular dynamics (MD) simulations. We provide direct estimates of the magnitude of internal bond rotation and the coupling between the polymer

segmental motion and the long-time component of anisotropy decay. Finally, based on these results, we propose a theoretical model for the reorientational relaxation mechanism of the PSC probe within a highly rigid polymer framework, offering a roadmap for using the PS IR-PP technique to accurately identify the FVEs associated with different reorientation timescales.

The remainder of this paper is structured as follows: Sec. II describes the MD simulation model and methodology. Section III presents the results and discussion, focusing on the influence of the potential of mean force (PMF) of the C_{Ph}–C_{Ph}–Se–CN dihedral on the simulated rotational anisotropy of the probes, the direct contribution of internal bond rotation to anisotropy decay, and the coupling between the simulated polymer segmental motion and the rotational motion of the probe molecule. Section IV introduces the theoretical framework of the rotational anisotropy mechanism of the probe, along with a brief calculation of FVEs sampled using the PSC probe. Finally, the key findings of this study are summarized in Sec. V.

II. METHODOLOGY AND SIMULATION DETAILS

A. Quantum chemical calculations

The potential energy surface (PES) scan for the PSC and DMPSC probes around the C_{Ph}–C_{Ph}–Se–CN dihedrals in an implicit PMMA polymer solvent (using the SMD solvation model[14]) was carried out at the B3LYP/6-311++G(D,P) level of theory, using Gaussian 16.[15]

B. Molecular dynamics simulations

To ensure a well-sampled phase space trajectory beyond the limitations of a standard MD protocol, ten different initial configurations were generated. Each configuration consisted of 12 PMMA chains dissolved with a single vibrational probe (PSC, DMPSC, or ClBZN), generated using the CHARMM-GUI package.[16,17] We selected PMMA chains built up with 100 monomer units as our representative polymer. The initial configurations of the polymer and the initial positions of the vibrational probes varied. Fixed-charge non-polarizable CHARMM force field parameters for the polymer were directly obtained from the CHARMM-GUI package, while the fftk package[18] was used to derive CHARMM force field parameters for the vibrational probes, particularly for site charges on heavy atoms and torsional parameters for the C_{Ph}–C_{Ph}–Se–CN dihedral.

Classical MD simulations were performed with the Large-scale Atomic/Molecular Massively Parallel Simulator (LAMMPS) package.[19] Energy-minimized initial configurations, obtained via a conjugate gradient search algorithm, were subjected to a 10 ns NPT run at 300 K and 1 atm pressure using a Nosé–Hoover thermostat and barostat,[20] with 1 ps temperature and 2 ps pressure damping parameters, respectively. Subsequently, an NVT run on each density-equilibrated configuration was carried out at 300 K for 20 ns. The equations of motion were integrated using the Verlet method with a 2-fs time step. Bonds involving hydrogen atoms and angles flanked by two hydrogen atoms were constrained using the Self Holonomic Algorithm for Keeping Equilibrium (SHAKE) algorithm.[21] Periodic boundary conditions were applied in all three dimensions, and intra- and intermolecular interactions were calculated using the standard functional form of the CHARMM force field. Coordinates were stored with a 4-fs resolution to compute time correlation functions from the last 10 ns of NVT trajectories. To validate the derived force field parameters for the vibrational probes, the simulated density at 300 K and 1 atm for a system consisting of 256 PSC molecules was calculated to be 1.40 g/ml, in good agreement with the experimental value of 1.48 g/ml. The molecular van der Waals volumes and principal components of inertia for PSC and DMPSC are shown in Table I. The data clearly show that the larger inertia of DMPSC restricts its rotational motion, thereby reducing the anisotropy of the –SeCN unit to a greater extent than PSC.

TABLE I. van der Waals volumes and principal components of inertia for PSC, DMPSC, and ClBZN.

Probe	V_{vdW} (Å^3)	I_A (kg m^2)	I_B (kg m^2)	I_C (kg m^2)
PSC	131.55	3.46×10^{-45}	1.19×10^{-44}	1.24×10^{-44}
DMPSC	166.70	6.86×10^{-45}	1.26×10^{-44}	1.54×10^{-44}

To eliminate molecular size effects on the simulated rotational anisotropy, additional simulations were conducted on a series of configurations in PMMA with a PSC probe. In these simulations, the torsional coefficients around the C_{Ph}–C_{Ph}–Se–CN dihedral were adjusted to mimic the potential energy barrier for DMPSC around the same dihedral, while keeping the atomic site charges and Lennard-Jones parameters unchanged. This modified PSC model will be referred to as "mimic DMPSC." Furthermore, to decouple the timescale of the internal rotation of the –SeCN unit around the C_{Ph}–Se bond from the overall molecular rotation, a set of simulations was performed with PSC and DMPSC, where the phenyl ring atoms were kept frozen (by initializing the ring atom velocity components to zero and setting the computed force components on each of the ring atoms to zero at each time step), while allowing the remaining bath atoms (the polymer and the –SeCN unit) to move. These model simulations will be referred to as "frozen ring" systems in the following.

III. RESULTS AND DISCUSSIONS

A. Potential energy surface of internal bond rotation

Since ClBZN lacks internal bond rotation that could affect the rotational anisotropy of the CN bond vector, our analysis focuses on the PSC and DMPSC molecules. The torsional barrier for the internal rotation of the –SeCN moiety around the C_{Ph}–C_{Ph}–Se–CN dihedral, derived from B3LYP/6-311++G(D,P) calculations with an implicit PMMA solvent, is shown in Fig. 1(a). The molecular structures of the vibrational probes and the C_{Ph}–C_{Ph}–Se–CN dihedrals (highlighted in orange) subjected to the potential energy surface (PES) scan are displayed next to their respective potential curves. For PSC, the estimated barrier height for internal rotation is 2.78 kJ/mol, which is slightly above the thermal energy at room temperature. In contrast, methylation at the ortho positions of the phenyl rings increases this barrier height to 19.66 kJ/mol for DMPSC. These quantum chemical (QC) calculations indicate that increased steric crowding at the ortho positions results in higher activation energy for the –SeCN group to rotate around the C_{Ph}–C_{Ph}–Se–CN dihedral. Since the torsional barrier for PSC is close to the thermal energy at room temperature, calculations using an implicit solvent

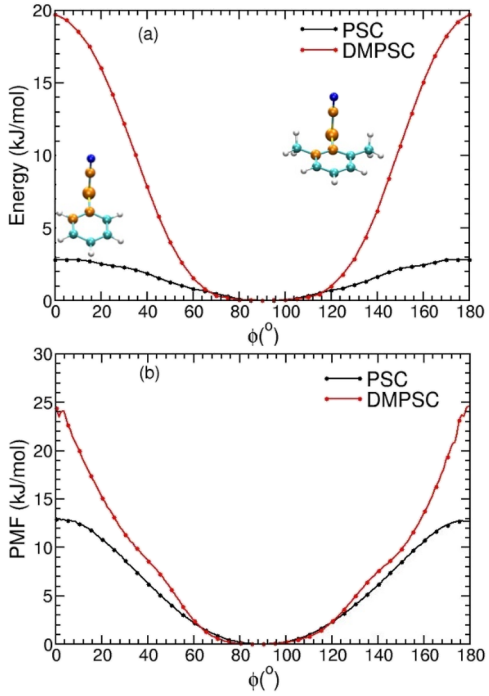

FIG. 1. Comparisons of (a) potential energy surfaces from B3LYP/6-311++G(D,P) calculations with the SMD model for PMMA and (b) potentials of mean forces (PMFs) calculated from the unbiased molecular dynamics trajectories for PSC and DMPSC in an explicit PMMA matrix for the internal rotation of the –SeCN moiety around the C_{Ph}–C_{Ph}–Se–CN dihedral.

model imply that the timescale for this internal bond rotation is likely fast compared to the wobbling motion of the probe, leading to a negligible contribution to the overall anisotropy decay of the –CN chromophore.

MD simulations provide a more realistic estimation of the potential energy barrier for internal bond rotation in an explicit PMMA solvent by calculating the potential of mean force (PMF) from the probability distribution $[P(\phi)]$ of the C_{Ph}–C_{Ph}–Se–CN dihedral angle (ϕ), relative to the maximum of the distribution $[P_{max}(\phi)]$,

$$PMF = k_B T \log \frac{P_{max}(\phi)}{P(\phi)}, \tag{5}$$

where k_B and T are the Boltzmann constant and temperature, respectively. Here, $P(\phi)$ is computed from the full dynamics of the probe molecule, sampling the maximum possible angular space due to internal bond rotation. Figure 1(b) shows a comparison of the potential barrier heights for the internal rotation of the –SeCN group around the phenyl ring for the two probes simulated in PMMA. Since these calculations were performed using unbiased MD trajectories, the PMFs cover only the range of dihedral angles sampled due to the internal rotation of the –SeCN unit. For PSC, the PMF samples the entire angular space around the dihedral, resulting in a barrier height ~6.0 times larger in the condensed phase compared to the quantum chemical (QC) PES results. In contrast, DMPSC, with symmetric ortho substitutions, exhibits a large torsional barrier height of 24.45 kJ/mol, which is about 1.24 times larger than the value obtained from QC PES scans. This indicates that the PMF of internal bond rotation in PSC is more sensitive to the free volume element (FVE) interacting with the –SeCN unit due to explicit atomistic interactions with the polymer matrix, whereas the PMF of DMPSC is predominantly influenced by intramolecular steric interactions. The comparison of PMFs between PSC and DMPSC suggests that the rate of internal bond rotation decreases with increasing steric effect. Further discussion of the simulated rotational anisotropy across these probes will provide additional insights into this aspect.

B. Simulated rotational anisotropy

The rotational anisotropy of the CN bond vector is described by the second Legendre polynomial $C_2(t)$ as

$$C_2(t) = \frac{\langle 3\cos^2\theta - 1\rangle}{2}, \tag{6}$$

where θ is the angle between the unit vector along the CN bond at two different times. Figure 2(a) shows a comparison of the computed $C_2(t)$ for the investigated probes: PSC, DMPSC, ClBZN, and "mimic DMPSC." For the PSC variants, the computed $C_2(t)$ values are fitted with the double exponential function, including an instantaneous

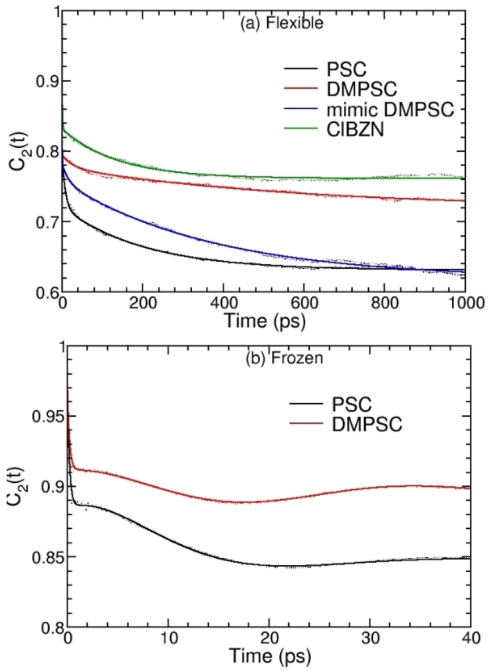

FIG. 2. Simulated rotational anisotropy of the CN bond vector of PSC, DMPSC, and ClBZN with (a) flexible phenyl ring and (b) frozen phenyl ring consideration in PMMA. The TCF data are shown as dots, while the solid lines represent the fit to the data.

TABLE II. Fit parameters of simulated $C_2(t)$ with flexible models of the probes.

Probe	a_1	$\delta(t)$ (ps)	a_2	τ_1 (ps)	a_3	τ_2 (ps)	a_4
PSC	0.23	0.30	0.08	7.85	0.09	202.5	0.63
DMPSC	0.23	0.44	0.02	27.71	0.06	606.6	0.72
Mimic DMPSC	0.19	0.47	0.03	15.01	0.14	380.2	0.62
ClBZN	⋯	⋯	0.10	1.05	0.07	137.28	0.76

decay component, which is modeled as a Dirac δ-function for this ultrafast inertial decay component,

$$C_2(t) = a_1\delta(t) + a_2e^{-t/\tau_1} + a_3e^{-t/\tau_2} + a_4. \quad (7)$$

The $\delta(t)$ component is obtained from a single exponential fit to the initial 1 ps component of $C_2(t)$. While fitting the time correlation functions (TCFs) with a double exponential function, the $\delta(t)$-component is kept constrained. For ClBZN, $C_2(t)$ is best fitted with a double exponential function and an offset. The fits extend until $C_2(t)$ reaches a plateau value, which in all cases samples the time domain significantly beyond the vibrational lifetimes of the probes. The fitted parameters for the different probe molecules are tabulated in Table II.

Figure 2(a) shows that the simulated $C_2(t)$ decays more slowly with increasing methyl crowding at the ortho positions, from PSC to DMPSC. The τ_1 values in Table II, corresponding to the faster dynamics of the PSC variants, are in good agreement with the experimental values of 4.6 and 31.9 ps, respectively. For the "mimic DMPSC" model, $C_2(t)$ decays more slowly than in PSC, yielding a τ_1 value twice that of PSC. Thus, an increase in the torsional barrier, whether due to steric crowding at the ortho positions of the phenyl ring or adjustments in the torsional parameters ("mimic DMPSC"), impedes the rotation of the SeCN unit around the C_{Ph}–Se bond. The simulated longer time constant, τ_2, matches well with the experimental values for PSC (229.3 ps) but is twice as large as the experimental value for DMPSC (284.5 ps). This discrepancy may stem from limitations in force field-based simulations. Notably, the τ_2 value for the "mimic DMPSC" is nearly twice that of PSC, suggesting a difference in the magnitude of mean-squared torques experienced by the flexible PSC compared to its conformationally more rigid analog, "mimic DMPSC."

For ClBZN, the τ_1 value corresponds to the inertial dynamics of the molecule, while τ_2 represents the timescale for the WIAC motion inside the cage. $C_2(t)$ for ClBZN decays more slowly than for the PSC variants, which is surprising given that ClBZN has the smallest molecular size (V_{vdW} = 115.10 Å^3) among these probes. A similar scenario was observed in PS IR-PP experiments, where $r(t)$ decayed less for ClBZN than for PSC in polystyrene.[11] This observation can be attributed to the presence of internal bond rotation in PSC variants, leading to a faster decay of $C_2(t)$ compared to ClBZN, where the WIAC motion is the only mechanism of anisotropy decay.

To decouple the timescale of the internal bond rotation of the –SeCN unit around the C_{Ph}–C_{Ph}–Se–CN dihedral from the overall molecular rotation, we analyzed the computed $C_2(t)$ of the CN bond vector using "frozen ring" simulations, as shown in Fig. 2(b). The computed $C_2(t)$ exhibits an oscillatory behavior starting from 20 ps, indicating the limiting value of $C_2(t)$ due to the librational motion of the –SeCN unit. These TCFs were fitted using a damped oscillator model,

$$C_2(t) = a_1\delta(t) + a_2e^{-t/\tau_1}\cos\left(\frac{2\pi t}{T} - \phi\right) + a_3, \quad (8)$$

where T and ϕ are the period and the phase angle, respectively, as listed in Table III. The $C_2(t)$ in Fig. 2(b) decays at a slower rate as steric crowding at the ortho positions of the phenyl ring increases, similar to the behavior observed in the fully flexible model of the probes. The tabulated τ_1 values of this "frozen ring" model closely match those of the fully flexible model of a given probe, consistent with the PMF of internal bond rotation discussed earlier. The limiting anisotropy value a_3 for PSC, corresponding to an angular space sampling magnitude of ~18.0°, aligns closely with experimental results. This observation suggests that the internal rotation of the –SeCN unit around the C_{Ph}–C_{Ph}–Se–CN dihedral plays a significant role in the rapid decay of the rotational anisotropy of the –CN bond vector in the vibrational probes.

TABLE III. Fit parameters of simulated $C_2(t)$ with "frozen ring" models of the probes.

Probe	a_1	$\delta(t)$ (ps)	a_2	τ_1 (ps)	ϕ	T (ps)	a_3
PSC	0.10	0.2	0.05	9.68	57.4	40.60	0.85
DMPSC	0.07	0.2	0.02	24.52	56.9	33.70	0.90

C. Influence of polymer segmental motion

Previous studies[8,9] suggested that the longer time component of $C_2(t)$ for the transition dipole moment vector of PSC in PMMA is related to the constraint release mechanism due to the dynamics of the polymer backbone side chains. This mechanism allows increased angular space sampling by the WIAC motion of the probe. In this study, we attempt to compare the timescale of the polymer segmental motion with τ_2 from the simulated $C_2(t)$ for PSC.

We modeled the polymer segmental motion using the computed mean square displacement $[\Delta R^2(t)]$ of the center of mass (COM) of individual monomer units ($\mathbf{r}_i$) in the COM frame of the polymer chain.[22,23] This is given by

$$\Delta R^2(t) = \left\langle |\boldsymbol{r}_i(t) - \boldsymbol{r}_i(0)|^2 \right\rangle, \quad (9)$$

where $\boldsymbol{r}_i(t)$ and $\boldsymbol{r}_i(0)$ are the position vectors of the ith monomer at time t and zero, respectively. Figure 3(a) presents the calculated $\Delta R^2(t)$ for the COM of the monomers in PMMA. The monomers barely move beyond 1.0 Å over a timescale of 50 ns. We fitted the computed $\Delta R^2(t)$ using a slightly modified Rouse model,[23]

$$\Delta R^2(t) = at^\beta + \frac{2\langle R_e^2\rangle}{\pi^2}\sum_{p=1}^{N-1}\frac{1 - e^{-p^2t/\tau_R}}{p^2}, \quad (10)$$

where the short-time behavior of $\Delta R^2(t)$ is proportional to t^β and the long-time behavior is described by the collective Rouse relaxation of $N-1$ eigenmodes associated with the COM positions of the monomers [$r_i(t)$] in the polymer chain, which consists of N beads.[23] $\langle R_e^2\rangle$ in the equation represents the mean square

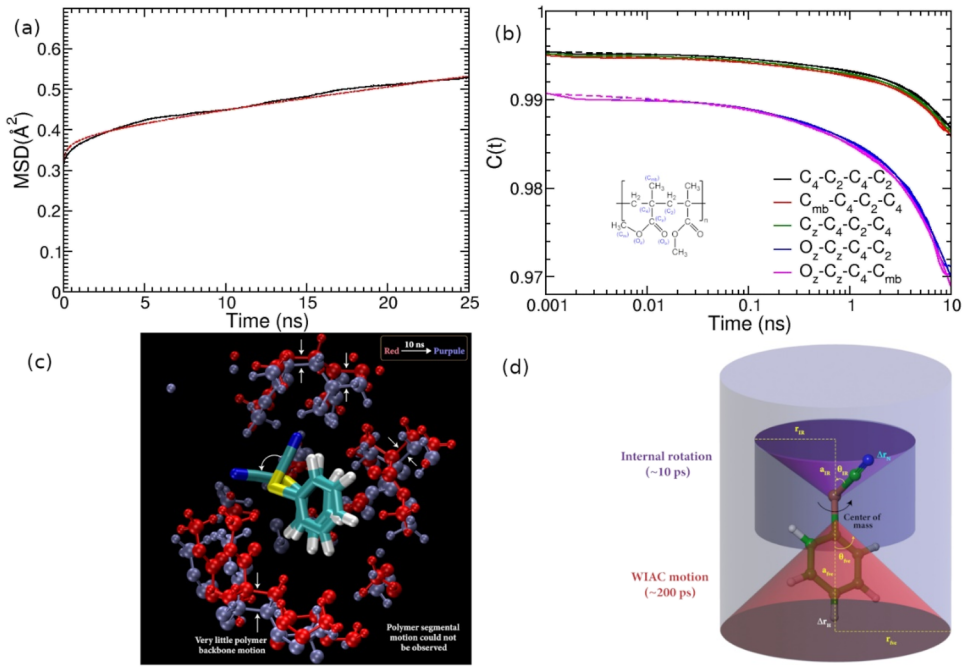

FIG. 3. (a) Calculated mean square displacement of the COM of monomers (black) along with the Rouse model fit (red) of the PMMA chains, (b) dihedral relaxation TCFs for selected dihedrals in the PMMA chain (the dashed lines represent raw data, while the solid lines represent the fits), (c) snapshot of PMMA segments within 6.0 Å of the COM of PSC are superimposed at time zero and after 10 ns, and (d) schematic of the proposed model for the WIAC motion of PSC in PMMA.

end-to-end separation of the polymer chains (1154.13 Å^2). We obtained a reasonable fit of $\Delta R^2(t)$ by using the above equation, yielding a = 0.3691 Å^2, β = 0.0368, and a characteristic Rouse time $\tau_R \approx 5.0$ ms. This large τ_R suggests that the monomers of the PMMA chains remain almost static during the reorientational relaxation time (τ_2) for all the probes studied here.

To explore the dynamics of various side chains of PMMA, we investigated the relaxation kinetics around specific dihedrals along the polymer chain by computing the following TCF:

$$C(t) = \langle \cos \delta\phi(t) \rangle, \tag{11}$$

where $\delta\phi(t)$ is the difference in dihedral angle around a given dihedral over the time interval t.

This TCF directly estimates the timescale for the relative motion of the first and fourth atoms about that dihedral. These TCFs were fitted using a tri-exponential function with an offset to extract both short- and long-time behaviors, as described by Eq. (7). Figure 3(b) displays TCFs for selected dihedrals (see the labels inside the plot) and their fits. The timescales from the fit parameters are listed in Table IV. None of the TCFs decay more than 4% over an elapsed time of 10 ns. The longest timescales (τ_3) associated with these TCFs range from 17 to 35 ns, which are significantly larger than the slow time component (~200 ps) of the simulated $C_2(t)$ for PSC.

Figure 3(c) further shows that the PMMA segments within 6.0 Å of the PSC COM are relatively static over time. Based on the Rouse time and torsional relaxation calculations, we conclude that the polymer segmental motions have a minimal impact on the longer timescale of the WIAC motion for the PSC probe.

TABLE IV. The fit parameters correspond to the selective dihedral relaxation for PMMA.

Dihedral	τ_1 (ns)	τ_2 (ns)	τ_3 (ns)
C4–C2–C4–C2	3.39×10^{-4}	0.167	29.73
C*mb*–C4–C2–C4	3.36×10^{-4}	0.182	35.22
C*z*–C4–C2–C4	3.40×10^{-4}	0.176	32.26
O*z*–C*z*–C4–C2	3.74×10^{-4}	0.246	17.60
O*z*–C*z*–C4–C*mb*	3.91×10^{-4}	0.271	20.89

IV. REVISITING THE WIAC MODEL

The preceding analyses lead us to conclude that the shorter time component (τ_1) of $C_2(t)$ for PSC in PMMA is significantly contributed by the internal bond rotation of the –SeCN unit around the C_{Ph}–C_{Ph}–Se–CN dihedral, whereas the longer timescale (τ_2) is minimally influenced by the constraint release mechanism involving the polymer segmental motions. Consequently, we propose to refine the WIAC model for the rotational anisotropy of the –SeCN unit in PSC within PMMA by associating different components of its motion with potential mechanistic pathways, as outlined in Secs. IV A–IV F.

A. Quantitative analyses of anisotropy decays

Kinosita *et al.*[24] and, later, Lipari and Szabo[7] developed the diffusion-in-a-cone (DIAC) model to describe the fluorescence emission anisotropy of rod-shaped cylindrical fluorophores in a membrane. This model assumes that the probe diffuses freely

("wobbles") within a cone with a half-angle ϑ, meaning that the equilibrium orientational distribution function with respect to the polar angle θ is constant for $0 \le \theta \le \vartheta$ and zero otherwise. Due to molecular symmetry, the orientational distribution function is assumed to be independent of the azimuthal angle. Similarly, as shown in Refs. 8 and 9, the orientational relaxation dynamics of the CN group in PSC trapped inside the polymer matrix can be described as WIAC motions with varying timescales, reflecting the spatial confinement and limited flexibility of the polymer backbones and side chains, which restrict the rotational motions of each probe molecule in a given free volume.

B. Inertial dynamics at short times

The experimentally measured initial anisotropy deviates from the ideal value of 0.4. This is explained by the fact that the inertial dynamics of the CN group is very fast, making it impossible to measure its contribution to short-time anisotropy decay with IR laser pulses of ~100 fs duration. The inertial orientational relaxation of the IR probe can be modeled as a WIAC motion with a Dirac delta function-like decay, where the half-cone angle specifying the angular space of the inertial WIAC motion is denoted as θ_{inert}. Since the diffusive (wobbling) motion within the range of the polar angle, $0 \le \theta \le \theta_{inert}$, is free, the normalized orientational distribution function is

$$P_{inert}(\theta) = \frac{1}{2\pi(1-\cos\theta_{inert})}, \quad 0 \le \theta \le \theta_{inert}, \\ = 0, \quad otherwise. \tag{12}$$

Then, the limiting anisotropy and the inertial contribution to $r(t)$ are given by

$$C_{2,inert}(t) = S_{inert}^2 + (1 - S_{inert}^2)\delta(t), \tag{13}$$

where the associated order parameter S_{inert} is

$$S_{inert} = \frac{1}{2}\cos\theta_{inert}(1+\cos\theta_{inert}). \tag{14}$$

The limiting anisotropy due to the inertial WIAC motion is S_{inert}^2. Measuring this order parameter provides direct information on the cone semi-angle θ_{inert}, which defines the radius of the cone or the associated FVE.

C. Internal rotation of CN group

The second component contributing to the anisotropy decay is the internal rotational relaxation of the CN group in the IR probe molecules. The CN group can undergo internal rotation around the single bond between the phenyl ring and the Se atom, affecting the decay of $r(t)$. The contribution of this internal rotation to the limiting anisotropy $r(\infty)$ can be calculated as follows: when internal rotational degrees of freedom are the only contributors to anisotropy decay, the orientational distribution function $P_{ir}(\theta)$ can be approximately written as

$$P_{ir}(\theta) = \frac{1}{2\pi\sin\theta_0}\delta(\theta - \theta_0), \tag{15}$$

where $2\pi \sin\theta_0$ is the normalization constant. Using the properties of correlation functions, one can write $r(\infty)$ as

$$r(\infty) = \frac{2}{5}\langle P_2(\cos\theta)\rangle^2. \tag{16}$$

The average of $P_2(\cos\theta)$ over $P(\theta)$ can be calculated, and the limiting anisotropy associated with this internal rotational relaxation is given by

$$r(\infty) = \frac{2}{5}(P_2(\cos\theta_0))^2. \tag{17}$$

Considering the chemical structure obtained from a density functional theory (DFT)-level calculation of PSC, the angle θ_0, which is the angle between the bond axis of C_{Ph}–Se and the CN bond axis, is ~72°. However, this angle (72°) for calculating $r(\infty)$ should be adjusted since the phenyl group in PSC is not infinitely heavier than the CN group. Thus, the effective angle θ_0 could be smaller than 72° and can be estimated experimentally by measuring the limiting anisotropy $r(\infty)$ associated with this internal rotation together with Eq. (17).

The time-dependence of $r(t)$ from the internal rotation of the CN group cannot be described by a diffusion equation of rotating objects in a two-dimensional space due to potential energy barriers along the internal rotational coordinate. Therefore, it is difficult to obtain an analytical expression for the time-dependent part of $r(t)$ in terms of the associated rotational diffusion constant, the viscosity of the local environment, and potential energy barrier heights. A convenient approximate expression for $r(t)/r(0)$ resulting from this internal rotational motion is an exponential function, i.e.,

$$C_{2,ir}(t) = (P_2(\cos\theta_0))^2 + \left(1 - (P_2(\cos\theta_0))^2\right)\exp(-t/t_{ir}), \tag{18}$$

where t_{ir} denotes the decay time constant associated with the internal rotational relaxation. Defining the associated order parameter as

$$S_{ir} = P_2(\cos\theta_0), \tag{19}$$

one can rewrite Eq. (18), similar to Eq. (13), as

$$C_{2,ir}(t) = S_{ir}^2 + \left(1 - S_{ir}^2\right)\exp(-t/t_{ir}). \tag{20}$$

D. Wobbling-in-a-cone motion of PSC as a rod-shaped object

If PSC molecules are situated in void spaces (FVEs) where they can freely wobble (diffuse) in a space approximated as a cone, and if the internal rotation of the CN group is much faster than this wobbling motion of PSC as a whole, we can model a single PSC as a rigid rod with cylindrical symmetry. In this limiting case, one can assume that the effective vibrational transition dipole unit vector, which is the average of the CN group's $\hat{\mu}$ over $P_{ir}(\theta)$, is coaxial with the molecular axis parallel to the (Ph)C–Se bond vector. Therefore, the WIAC motion of a rod-shaped molecule needs to be considered for describing its contribution to $r(t)$. Using the standard WIAC model, we have

$$C_{2,fve}(t) = S_{fve}^2 + \left(1 - S_{fve}^2\right)\exp\left(-t/t_{fve}\right), \tag{21}$$

where t_{fve} is the average relaxation time constant of the rod-shaped IR probe molecules in FVEs and the corresponding order parameter is related to the cone half-angle of the FVE as

$$S_{fve} = \frac{1}{2}\cos\theta_{fve}\left(1+\cos\theta_{fve}\right). \tag{22}$$

E. Total anisotropy decay

We defined three different order parameters associated with various reorientation processes. By definition, each order parameter reflects the extent of anisotropy decay associated with its respective process. Assuming that the three relaxation processes occur independently, the total correlation function $C_2(t)$ is the product of the three correlation functions, i.e.,

$$\begin{aligned} C_2(t) &= C_{2,inert}(t)C_{2,ir}(t)C_{2,fve}(t) \\ &= \left\{S_{inert}^2 + \left(1-S_{inert}^2\right)\delta(t)\right\}\left\{S_{ir}^2 + \left(1-S_{ir}^2\right)\exp\left(-t/t_{ir}\right)\right\} \\ &\quad\times\left\{S_{fve}^2 + \left(1-S_{fve}^2\right)\exp\left(-t/t_{fve}\right)\right\}. \end{aligned} \tag{23}$$

When the two decay time constants are substantially different, i.e., $t_{ir} \ll t_{fve}$, one can rewrite Eq. (23) approximately as

$$\begin{aligned} C_2(t) \cong{}& \left(1-S_{inert}^2\right)\delta(t) + S_{inert}^2\left(1-S_{ir}^2\right)\exp\left(-t/t_{ir}\right) \\ &+ S_{inert}^2 S_{ir}^2\left(1-S_{fve}^2\right)\exp\left(-t/t_{fve}\right) + S_{inert}^2 S_{ir}^2 S_{fve}^2. \end{aligned} \tag{24}$$

Comparing Eq. (24) with our fit function in Eq. (7), we find that the amplitudes of the four terms in Eq. (7) can be related to the order parameters as

$$\begin{aligned} a_1 = 1-S_{inert}^2,\ a_2 = S_{inert}^2\left(1-S_{ir}^2\right),\ a_3 = S_{inert}^2 S_{ir}^2\left(1-S_{fve}^2\right), \\ a_4 = S_{inert}^2 S_{ir}^2 S_{fve}^2. \end{aligned} \tag{25}$$

F. Association of FVEs with different rotational timescales of PSC in PMMA using experimental half-cone angles

To relate the FVEs to different rotational timescales of PSC in PMMA, we summarize key findings from this simulation study and recent experimental work.[11,13] Our computational findings indicate that the faster rotational anisotropy of the PSC probe, observed on a timescale of ~10 ps, is associated with instantaneous inertial dynamics and internal bond rotation of the –SeCN unit. This process samples the angular space around it (θ_{IR}), as illustrated in violet in Fig. 3(d). An earlier computational study on the isomerization dynamics of n-butane in the condensed phase also found a direct relationship between conformational population and cavity distribution around the flexible conformer.[25] In addition, recent time-resolved IR spectroscopy of 1,2-disubstituted ethyl radical derivatives showed that gauche-to-anti-isomerization reactions involving carbon–carbon single bond rotation at room temperature occur with a very slow timescale of about 35–45 ps.[26] Furthermore, using a series of –CN containing vibrational probes with varying internal bond rotations, PS IR-PP experiments identified a similar FVE sampled by the θ_{01} angular space inside the FVE in polystyrene polymer.[11] Given the similar values for θ_{IR} and θ_{01}, we propose that the fast rotational anisotropy decay is governed by a complex relaxation mechanism involving coupled angular space sampling by internal bond rotation and WIAC motion.

This finding highlights the complexity of rotational dynamics in specific systems and suggests that when internal rotational fluctuations are present and the barrier height exceeds the thermal energy at room temperature, they can significantly influence the short-time anisotropy dynamics of the probe molecules within the polymer matrix.

Another notable observation is that the simulated TCFs corresponding to the segmental relaxation of PMMA decay by only about 1% within an ~200 ps timescale, indicating that the WIAC-type diffusive dynamics of the IR probe have not yet begun in this regime. The longer-time rotational anisotropy decay of the PSC probe in PMMA, at ~200 ps, associated with the WIAC motion, probes the available angular space (θ_{fve}), depicted in cyan in Fig. 3(d). This angular space remains essentially unchanged in size and shape within this time regime, as supported by MD simulations, contrary to previous studies where the longer timescale (~200 ps) anisotropy decay of the PSC probe was attributed to FVE size and shape fluctuations inside the polymer matrix due to the constraint release mechanism involving structural rearrangement of the side-chain functional groups. Our study shows that the long-timescale orientational relaxation of the PSC probe reflects the static FVEs of the polymer. Therefore, we equate the average cone half-angle parameters $\langle\theta_{IR}\rangle = 22.1^\circ$ and $\langle\theta_{fve}\rangle = 28.6^\circ$ with two different sets of a and Δr values to estimate the respective FVE sizes. For the FVE sampled by the internal bond rotation of the –SeCN unit, a is the distance between the Se and N atoms of the PSC molecule (~3.02 Å obtained from the optimized structure) and Δr is the N atom's van der Waals radius (1.55 Å). This set of parameters yields an average FVE radius of 2.69 Å. We should note that this value is quite close to the FVE radius obtained from PS IR-PP experiments. Similarly, for the FVE corresponding to the total angular space sampled by the WIAC motion of the probe, a is the distance from the terminal p-hydrogen atom of the phenyl ring of the PSC molecule to its COM (4.31 Å) and Δr is the van der Waals radius of the p-hydrogen atom (1.2 Å), which yields an average FVE radius 3.26 Å. This FVE is ~11% larger than the van der Waals volume (V_{vdW}) of PSC, a reasonable estimation since the FVE sampled by the probe should be at least equal to or larger than its actual van der Waals volume.

V. SUMMARY AND CONCLUSIONS

In this work, we proposed a modified version of the wobbling-in-a-cone (WIAC) model for the rotational anisotropy of PSC embedded in PMMA, based on the key findings from classical MD simulations. The simulated $C_2(t)$ for PSC and DMPSC in PMMA reveals a systematic slowing down of both shorter and longer time components. The shorter time component is likely influenced by the increased relative free energy barrier for the internal rotation of the –SeCN moiety around the C_{Ph}–C_{Ph}–Se–CN dihedral as substituent crowding around the dihedral increases. "Frozen ring" simulations quantitatively demonstrate that this shorter time

component is primarily due to the internal bond rotation process. The Rouse relaxation time associated with the $\langle \Delta R^2(t) \rangle$ of the monomers in PMMA falls within the millisecond regime, implying that the polymer backbones remain almost static on the timescale of the longer-time behavior of the simulated $C_2(t)$ for all the probes. For selected dihedrals along the PMMA backbone, the torsional relaxation processes of backbones contribute to the anisotropy decay by only about 4%, with the longest time constant ranging from 17 to 35 ns. These findings indicate that the polymer segmental motion plays a minimal role in the longer-time wobbling motion of the probes. Based on these observations, we propose that the faster rotational anisotropy of the PSC probe within an ~10 ps timescale is associated with the internal bond rotation of the –SeCN unit, sampling the angular space around it (θ_{IR}), while the longer time component of $C_2(t)$ is associated with the WIAC motion, probing the available angular space (θ_{fve}).

To ensure a more accurate analysis of the FVE size and distribution, it is crucial to develop and use IR probes that do not have any internal rotation but have a long vibrational lifetime. Such probes will provide a clearer picture of the long-time WIAC motion, which likely samples the static FVEs of the polymer. Ultimately, the initial void space sampled by internal rotational fluctuations may be less relevant to the actual physical FVEs of the polymer, which can only be accurately probed by the long-time WIAC motion.

ACKNOWLEDGMENTS

This work was supported by the Institute for Basic Science (Grant No. IBS-R023-D1) (M.C.) and a National Research Foundation of Korea (NRF) grant funded by the Korean government (MSIT) (Grant Nos. NRF-2020R1A2C2010675 and NRF-2020R1A5A1019141) (K.K.).

AUTHOR DECLARATIONS

Conflict of Interest

The authors have no conflicts to disclose.

Author Contributions

Sourav Palchowdhury: Conceptualization (equal); Data curation (equal); Formal analysis (equal); Investigation (equal); Methodology (equal); Software (equal); Validation (equal); Visualization (equal); Writing – original draft (equal); Writing – review & editing (equal). **Saptarsi Mondal**: Conceptualization (supporting); Formal analysis (equal); Investigation (supporting); Software (supporting); Writing – original draft (supporting); Writing – review & editing (supporting). **Kyungwon Kwak**: Conceptualization (equal); Formal analysis (equal); Investigation (equal); Project administration (equal); Supervision (equal); Validation (equal); Writing – original draft (equal); Writing – review & editing (equal). **Minhaeng Cho**: Conceptualization (equal); Formal analysis (equal); Funding acquisition (lead); Investigation (equal); Project administration (equal); Resources (lead); Supervision (equal); Validation (equal); Writing – original draft (equal); Writing – review & editing (equal).

DATA AVAILABILITY

The data that support the findings of this study are available from the corresponding author upon reasonable request.

REFERENCES

[1] K. Mukherjee, S. Palchowdhury, and M. Maroncelli, "Do electrostatics control the diffusive dynamics of solitary water? NMR and MD studies of water translation and rotation in dipolar and ionic solvents," J. Phys. Chem. B **128**, 3689–3706 (2024).

[2] S. Palchowdhury, K. Mukherjee, and M. Maroncelli, "What do far-infrared spectra of solitary water in 'water-in-solvent' systems reveal about water's solvation and dynamics?," J. Chem. Phys. **159**, 034502 (2023).

[3] G. S. Jas, E. J. Larson, C. K. Johnson, and K. Kuczera, "Microscopic details of rotational diffusion of perylene in organic solvents: Molecular dynamics simulation and experiment vs Debye–Stokes–Einstein Theory," J. Phys. Chem. A **104**, 9841–9852 (2000).

[4] N. Brilliantov, V. Denisov, and P. Krapivsky, "Generalized Stokes-Einstein-Debye relation for charged Brownian particles in solution," Physica A **175**, 293–304 (1991).

[5] G. Lipari and A. Szabo, "Model-free approach to the interpretation of nuclear magnetic resonance relaxation in macromolecules. 1. Theory and range of validity," J. Am. Chem. Soc. **104**, 4546–4559 (1982).

[6] K. Kinosita, Jr., A. Ikegami, and S. Kawato, "On the wobbling-in-cone analysis of fluorescence anisotropy decay," Biophys. J. **37**, 461–464 (1982).

[7] G. Lipari and A. Szabo, "Effect of librational motion on fluorescence depolarization and nuclear magnetic resonance relaxation in macromolecules and membranes," Biophys. J. **30**, 489–506 (1980).

[8] S. M. Fica-Contreras, D. J. Hoffman, J. Pan, C. Liang, and M. D. Fayer, "Free volume element sizes and dynamics in polystyrene and poly(methyl methacrylate) measured with ultrafast infrared spectroscopy," J. Am. Chem. Soc. **143**, 3583–3594 (2021).

[9] D. J. Hoffman, S. M. Fica-Contreras, and M. D. Fayer, "Amorphous polymer dynamics and free volume element size distributions from ultrafast IR spectroscopy," Proc. Natl. Acad. Sci. U. S. A. **117**, 13949–13958 (2020).

[10] C. Wästlund and F. H. J. Maurer, "Positron lifetime distributions and free volume parameters of PEO/PMMA blends determined with the maximum entropy method," Macromolecules **30**, 5870–5876 (1997).

[11] J. Pan, A. P. Charnay, S. M. Fica-Contreras, and M. D. Fayer, "Restricted orientation anisotropy method for FVE radii characterization: Confirmed and refined via the study of six vibrational probes," Macromolecules **57**, 903–915 (2024).

[12] S. Mondal, S. Palchowdhury, K. Park, S. Sung, Y. H. Lee, K. Kwak, and M. Cho, "Revisiting the ultrafast IR spectroscopic study of free volume elements in polymers: The role of probe molecule's internal rotational fluctuation in anisotropy decays," chemRxiv:2023-q76kp (2023).

[13] A. P. Charnay, J. Pan, and M. D. Fayer, "Influence of internal bond rotation on ultrafast IR anisotropy measurements and the internal rotational potential," J. Phys. Chem. B **128**, 280–286 (2024).

[14] A. V. Marenich, C. J. Cramer, and D. G. Truhlar, "Universal solvation model based on solute electron density and on a continuum model of the solvent defined by the bulk dielectric constant and atomic surface tensions," J. Phys. Chem. B **113**, 6378–6396 (2009).

[15] M. J. Frisch, G. W. Trucks, H. B. Schlegel, G. E. Scuseria, M. A. Robb, J. R. Cheeseman, G. Scalmani, V. Barone, G. A. Petersson, H. Nakatsuji, X. Li, M. Caricato, A. V. Marenich, J. Bloino, B. G. Janesko, R. Gomperts, B. Mennucci, H. P. Hratchian, J. V. Ortiz, A. F. Izmaylov, J. L. Sonnenberg, D. Williams-Young, F. Ding, F. Lipparini, F. Egidi, J. Goings, B. Peng, A. Petrone, T. Henderson,

D. Ranasinghe, V. G. Zakrzewski, J. Gao, N. Rega, G. Zheng, W. Liang, M. Hada, M. Ehara, K. Toyota, R. Fukuda, J. Hasegawa, M. Ishida, T. Nakajima, Y. Honda, O. Kitao, H. Nakai, T. Vreven, K. Throssell, J. A. Montgomery, Jr., J. E. Peralta, F. Ogliaro, M. J. Bearpark, J. J. Heyd, E. N. Brothers, K. N. Kudin, V. N. Staroverov, T. A. Keith, R. Kobayashi, J. Normand, K. Raghavachari, A. P. Rendell, J. C. Burant, S. S. Iyengar, J. Tomasi, M. Cossi, J. M. Millam, M. Klene, C. Adamo, R. Cammi, J. W. Ochterski, R. L. Martin, K. Morokuma, O. Farkas, J. B. Foresman, and D. J. Fox, Gaussian 16, Revision B.01, 2016.

[16]Y. K. Choi, S.-J. Park, S. Park, S. Kim, N. R. Kern, J. Lee, and W. Im, "CHARMM-GUI polymer builder for modeling and simulation of synthetic polymers," J. Chem. Theory Comput. **17**, 2431–2443 (2021).

[17]S. Jo, T. Kim, V. G. Iyer, and W. Im, "CHARMM-GUI: A web-based graphical user interface for CHARMM," J. Comput. Chem. **29**, 1859–1865 (2008).

[18]C. G. Mayne, J. Saam, K. Schulten, E. Tajkhorshid, and J. C. Gumbart, "Rapid parameterization of small molecules using the force field toolkit," J. Comput. Chem. **34**, 2757–2770 (2013).

[19]S. Plimpton, "Fast parallel algorithms for short-range molecular dynamics," J. Comput. Phys. **117**, 1–19 (1995).

[20]D. J. Evans and B. L. Holian, "The Nose–Hoover thermostat," J. Chem. Phys. **83**, 4069–4074 (1985).

[21]J.-P. Ryckaert, G. Ciccotti, and H. J. C. Berendsen, "Numerical integration of the cartesian equations of motion of a system with constraints: Molecular dynamics of *n*-alkanes," J. Comput. Phys. **23**, 327–341 (1977).

[22]D. Diddens, A. Heuer, and O. Borodin, "Understanding the lithium transport within a rouse-based model for a PEO/LiTFSI polymer electrolyte," Macromolecules **43**, 2028–2036 (2010).

[23]A. Maitra and A. Heuer, "Cation transport in polymer electrolytes: A microscopic approach," Phys. Rev. Lett. **98**, 227802 (2007).

[24]K. Kinosita, Jr., S. Kawato, and A. Ikegami, "A theory of fluorescence polarization decay in membranes," Biophys. J. **20**, 289–305 (1977).

[25]D. Chandler, "Statistical mechanics of isomerization dynamics in liquids and the transition state approximation," J. Chem. Phys. **68**, 2959–2970 (1978).

[26]S. Park, J. Shin, H. Yoon, and M. Lim, "Rotational isomerization of carbon–carbon single bonds in ethyl radical derivatives in a room-temperature solution," J. Phys. Chem. Lett. **13**, 11551–11557 (2022).